

2002

Cyclotron frequency coupled enhancement of Kerr rotation in low refractive index-dielectric/magneto-optic bilayer thin-film structures

A. De
University of New Orleans

A. Puri
University of New Orleans

Follow this and additional works at: https://scholarworks.uno.edu/phys_facpubs



Part of the [Physics Commons](#)

Recommended Citation

J. Appl. Phys. 91, 9777 (2002)

This Article is brought to you for free and open access by the Department of Physics at ScholarWorks@UNO. It has been accepted for inclusion in Physics Faculty Publications by an authorized administrator of ScholarWorks@UNO. For more information, please contact scholarworks@uno.edu.

Cyclotron frequency coupled enhancement of Kerr rotation in low refractive index-dielectric/magneto-optic bilayer thin-film structures

A. De and A. Puri

Department of Physics, University of New Orleans, New Orleans, Louisiana 70148

(Received 18 December 2001; accepted for publication 22 February 2002)

We investigate the enhancement of magneto-optic polar Kerr rotation over a broad range of optical frequencies. The Drude model for the dielectric tensor is considered. Resonance-like peaks in the Kerr rotation and ellipticity caused in the vicinity of a plasma edge is extended throughout the visible spectrum by deriving an expression for the cyclotron frequency such that $\text{Re}(\epsilon_{xx}) \sim 1$ at any given incident photon energy and plasma frequency of the material. The Kerr rotation obtained by use of this expression was studied for the case of InSb and further enhancement of Kerr rotation was achieved in the case of LiF/InSb bilayer thin-film structure, grown on a glass substrate. The numerical analysis was carried out using a 2×2 characteristic matrix, which takes into account multiple reflections and interface effects within the medium. In addition the role of various magneto-optic material parameters and layer thicknesses is investigated in determining the optical frequency at which the maximum Kerr rotation occurs, under the present cyclotron frequency condition. Enhanced Kerr rotation greater than 1.5° over a broad range of optical frequencies was obtained. Tables showing optimum figure of merit for repeated LiF/InSb bilayers at 3.1 eV for different plasma frequencies are also provided. © 2002 American Institute of Physics. [DOI: 10.1063/1.1469665]

I. INTRODUCTION

In the last three decades a vast amount of research has been carried out in order to enhance the magneto-optic Kerr effect (MOKE), particularly because of its importance in the optical readout of magnetically stored information. The polar Kerr effect continues to be the preferred configuration for magneto-optic (MO) readout as most MO materials have perpendicular magnetization. The appearance of high peaks in the MOKE spectrum has been attributed to various physical origins such as interband transitions and spin-orbit coupling.^{1,2} Feil and Hass³ have suggested a slightly different explanation for large MOKE. They have shown through model calculations that large MOKE occurs where $\text{Re}(\epsilon_{xx}) \sim 1$, which is in the vicinity of plasma resonance frequency of free charge carriers.

Kerr rotation (KR) enhancement in the case of ferromagnetic layers embedded in metallic matrices has been more widely attributed to plasma resonance of free carriers in the nonmagnetic noble metals^{4,5} and also to sharp surface plasmon resonance of noble metals in total reflection geometry.⁶ It has also been reported⁷⁻⁹ that enhancement of KR is possible by deposition of a low refractive index dielectric (DE) film on top of the MO material. This has been attributed to the fact that the DE film would reduce the polarization component of the directly reflected light without influencing the component induced by the KR. In Ref. 10 it has been shown that such an enhancement of MOKE can be expected if the dielectric constants of neighboring materials are low and well matched to each other.

In this article we have carried out numerical simulations to enhance the KR in view of the concepts presented in Refs. 3 and 7-9. In particular we study the combined effect of

Kerr enhancement due to plasma resonance in the MO media and due to deposition of a low refractive index film on such a MO media. This is done for the particular case of LiF/InSb bilayer structures. We assume that macroscopically, MO effects of free carriers can be represented by the Drude model with reasonable accuracy and that large MOKE indeed occurs wherever $\text{Re}(\epsilon_{xx}) \sim 1$. This enables us to obtain a simple expression for the cyclotron frequency ω_c in the Drude model, which satisfies the Feil and Hass condition [i.e., $\text{Re}(\epsilon_{xx}) \sim 1$] at any optical frequency and thus enables us to obtain high KR at any optical frequencies of our choice, simply by adjusting the MO and dielectric layer thickness and by choosing an appropriate plasma frequency. Broadband characteristics in the KR can also be achieved. This has been carried out with particular reference to InSb, which was the chosen MO material and has been discussed in greater detail along with some theoretical background in Sec. II.

A 2×2 characteristic matrix formulation¹¹⁻¹³ which would be required to analyze multilayer structures, is briefly discussed in Sec. III. In Sec. IV, under the ω_c condition obtained in Sec. II, we were able to further enhance the KR, by depositing a low refractive index DE on top of the MO. We chose LiF as our DE as it has a very low refractive index. Various parameters such as plasma frequency (which depends on the doping density) and layer thickness were varied in order to investigate their respective effects on MOKE. It was found that the optical frequency at which the KR peaks is quite heavily dependent on the layer thickness of the DE and the MO material, which enabled us to control the MOKE to some extent by controlling layer thickness. The LiF/InSb bilayer structure was also studied by repeating it a number of times at an optical frequency of 3.1 eV. We have provided

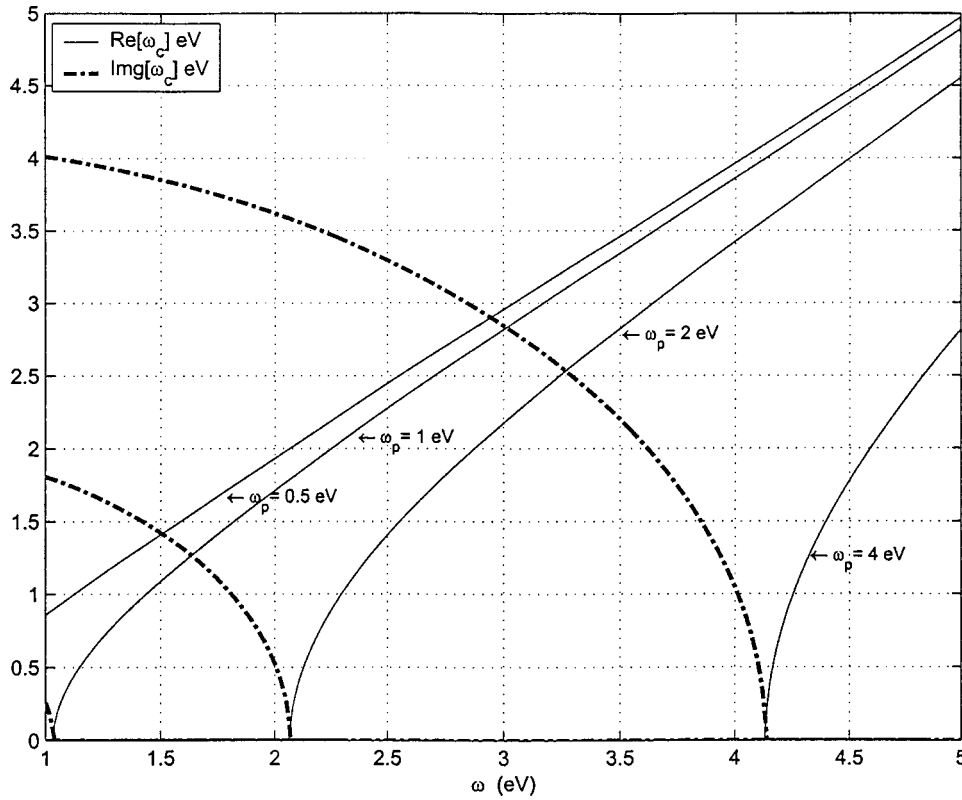


FIG. 1. Solution curves showing real and imaginary parts of ω_c for various values of ω_p .

tables that give us various MOKE parameters after having optimized the figure of merit (FOM).

II. BACKGROUND THEORY AND DERIVATION

Circularly polarized light propagating along the z axis can be expressed in terms of its electric field vector by

$$E_{\pm} = \text{real}\{E_0 e^{i(\omega t - 2\pi \tilde{n}_{\pm} z / \lambda_0)} (e_x \pm i e_y)\}, \tag{1}$$

where λ_0 is the wavelength in vacuum, and e_x and e_y are unit vectors in x and y directions, respectively. The $+$, $-$ signs represent right and left circularly polarized modes of propagation of an electromagnetic wave in a longitudinal magnetic field. \tilde{n}_{\pm} is the complex index of refraction given by $\tilde{n}_{\pm} = n_{\pm} - i k_{\pm}$, where n_{\pm} and k_{\pm} are the refractive and absorptive indices, respectively.

The dielectric tensor is in general complex and takes the form

$$\epsilon_{jk} = \epsilon_{1jk} + i \epsilon_{2jk}. \tag{2}$$

Symmetry of the problem configuration allows simplification of the dielectric tensor and it may be expressed as

$$\epsilon = \begin{pmatrix} \epsilon_{xx} & i \epsilon_{xy} & 0 \\ -i \epsilon_{xy} & \epsilon_{yy} & 0 \\ 0 & 0 & \epsilon_{zz} \end{pmatrix}. \tag{3}$$

It is well known that the dielectric response of the medium can be described by Maxwell's equations. Applying Maxwell's equations on electromagnetic fields given by Eq. (1) leads to the following expression for the complex index of refraction:

$$n^2 = \mu \epsilon. \tag{4}$$

Ignoring nonlinear effects in the material response and following the arguments of Landau *et al.* that $\mu = 1$ at optical frequencies, the complex index of refraction may thus simply be expressed as

$$(n - ik)_{\pm}^2 = \epsilon_{xx} \pm i \epsilon_{xy} = \epsilon_{\pm}. \tag{5}$$

The complex polar MO rotation and ellipticity of reflected light can be described by using the properties of the material's dielectric tensor by¹⁴

$$\theta_k - i \xi_k = \frac{\epsilon_{xy}}{(1 - \epsilon_{xx}) \sqrt{\epsilon_{xx}}}. \tag{6}$$

KR is described by the imaginary part of the off-diagonal matrix element ϵ_{xy} and Kerr ellipticity (KE) by the real part. The KR may be simplified and expressed as

$$\theta_k = \frac{p \cdot \epsilon'_{xy} + q \cdot \epsilon''_{xy}}{p^2 + q^2}, \tag{7}$$

where ϵ'_{xy} , ϵ''_{xy} are real and imaginary parts of the off-diagonal dielectric tensor, respectively. $p = \alpha(1 - \alpha^2 + \beta^2) + 2\alpha\beta^2$ and $q = (\alpha^2 - \beta^2 - 1) + 2\alpha^2\beta$, where $\hat{\alpha}$ and $\hat{\beta}$ are related to the diagonal part of the dielectric tensor by $\sqrt{\epsilon_{xx}} = \alpha - i\beta$.

On application of a magnetic field the plasma reflection edge splits into two edges, and the separation between the two minima increases linearly¹⁵ with the field. Hence the application of a magnetic field changes the complex index of refraction, inducing magnetic circular birefringence and mag-

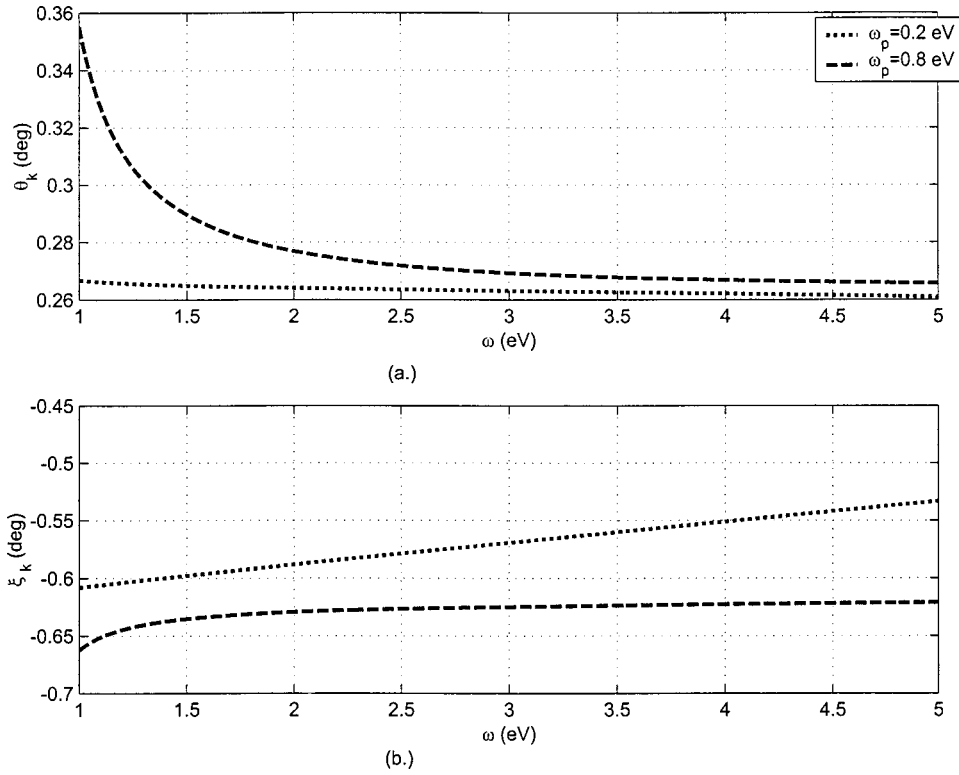


FIG. 2. (a) Kerr rotation and (b) Kerr ellipticity for bulk MO (01 arrangement).

netic circular dichroism. In the Kerr configuration with the pointing vector $\mathbf{S} \parallel \mathbf{B}_0$ and $\mathbf{E} \perp \mathbf{B}_0$ the complex dielectric tensor may be written¹⁶ as

$$\epsilon_{\pm} = \epsilon_{\infty} \left(1 - \frac{\omega_p^2}{\omega(\omega \pm \omega_c - i\nu)} \right), \quad (8)$$

where ω_p is the plasma frequency, ω_c is the cyclotron frequency, ν is the scattering frequency, and ϵ_{∞} is the background dielectric constant. The plasma frequency may be expressed as $\omega_p = (4\pi N e^2 / m^* \epsilon_c)^{1/2}$ and the cyclotron frequency as $\omega_c = H e / m^* c$. H being the magnetic field, c the speed of light, e the charge of an electron, m^* the effective mass, N the doping concentration, and ϵ_c the dielectric constant of the medium.

In a polar semiconductor material such as InSb, the MO effects would be altered when lattice vibrations are added. The changes will be largest in the vicinity of the optical phonon frequencies. Hence we may express the dielectric tensor as

$$\epsilon_{\pm} = \epsilon_{\infty} \left(1 - \frac{\omega_p^2}{\omega(\omega \pm \omega_c - i\gamma)} + \frac{\omega_L^2 - \omega_T^2}{(\omega_T^2 - \omega^2 + i\Gamma\omega)} \right), \quad (9)$$

where ω_L is the longitudinal phonon frequency, ω_T is the transverse phonon frequency, and Γ and γ are phonon damping constants.

An expression for the diagonal part of the dielectric tensor (ϵ_{xx}) can easily be obtained from Eqs. (5) and (9)

$$\epsilon_{xx} = \epsilon_{\infty} \left(1 - \frac{\omega_p^2(\omega - i\gamma)}{\omega((\omega - i\gamma)^2 - \omega_c^2)} + \frac{(\omega_L^2 - \omega_T^2)((\omega_T^2 - \omega^2) - i\Gamma\omega)}{(\omega_T^2 - \omega^2)^2 + \Gamma^2\omega^2} \right). \quad (10)$$

By solving the above equation for real and imaginary parts and ignoring γ^2 terms we obtain

$$\text{Re}(\epsilon_{xx}) = \epsilon_{\infty} \left(1 - \frac{\omega_p^2}{\omega^2 - \omega_c^2} + A \right), \quad (11)$$

where

$$A = \frac{(\omega_L^2 - \omega_T^2)(\omega_T^2 - \omega^2)}{(\omega_T^2 - \omega^2)^2 + \Gamma^2\omega^2}. \quad (12)$$

According to Ref. 7, a pronounced enhancement of the complex MOKE is expected in the vicinity of plasma resonance of free charge carriers which is in regions where $\text{Re}(\epsilon_{xx}) \sim 1$. Thus by substituting this condition in Eq. (11) we obtain an expression for ω_c

$$\omega_c = \sqrt{\omega^2 - \frac{\epsilon_{\infty}\omega_p^2}{\epsilon_{\infty}(1+A) - 1}} \quad (13)$$

and by setting $\text{Re}(\epsilon_{xx}) = 1$, Eq. (7) can simply be rewritten as follows:

$$\theta_k = \frac{1}{2} \left(\frac{\epsilon'_{xy}}{\sqrt{1 - \beta^2}} + \frac{\epsilon''_{xy}}{\beta} \right). \quad (14)$$

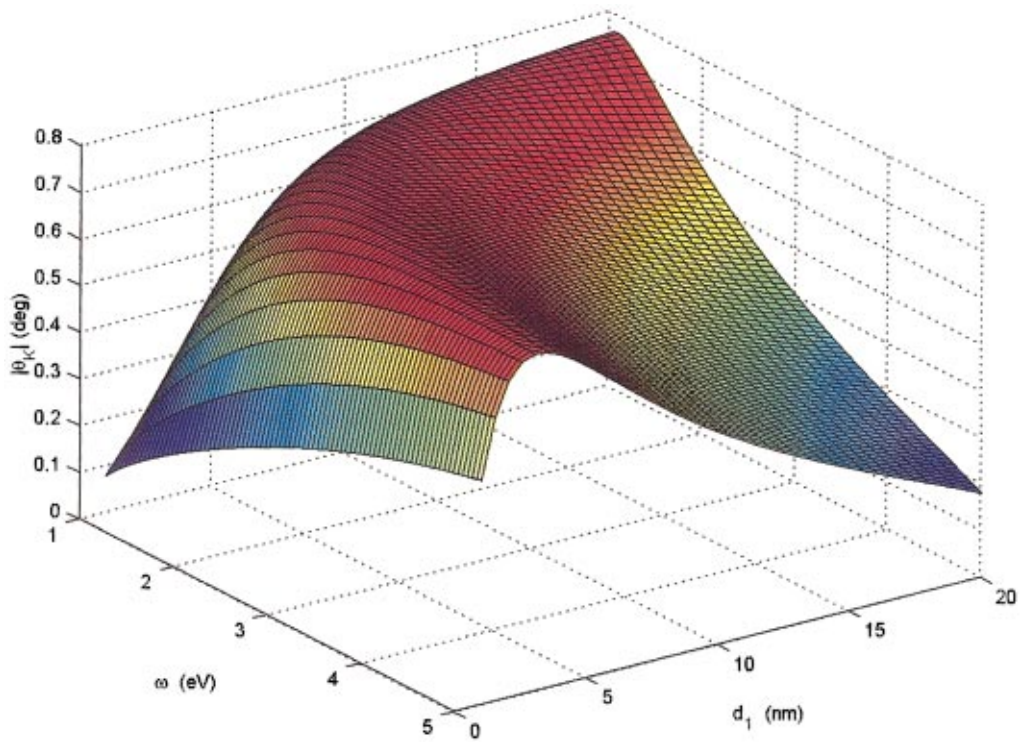


FIG. 3. (Color) Kerr rotation as a function of ω and d_1 at $\omega_p=0.8$ eV.

Expression (13) suggests if the cyclotron frequency (which is dependent on applied magnetic field and temperature) were made to vary as a function of incident photon energy and properties of the material such as plasma frequency (which depends on doping concentration) then a high and possibly flat KR could be obtained across the optical frequency spec-

trum of interest. We set a maximum upperbound limit for the plasma frequency in order to allow ω_c to have only real values. This constraining factor can be obtained from Eq. (13) and can be written as

$$((1+A) - 1/\epsilon_\infty)\omega^2 \geq \omega_p^2. \tag{15}$$

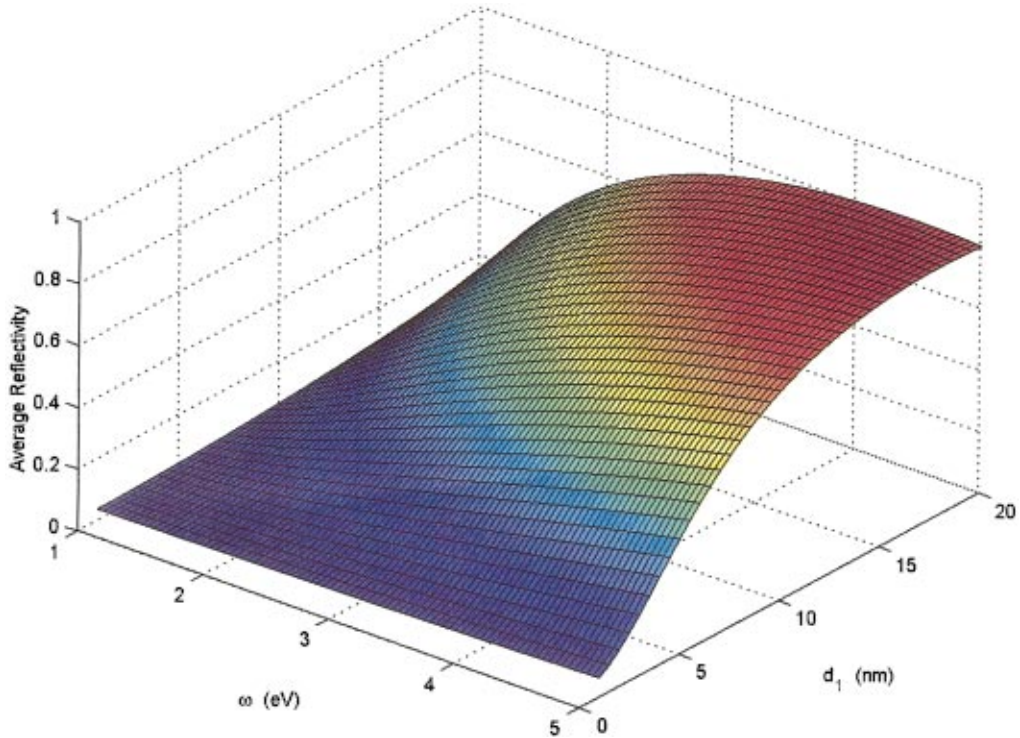


FIG. 4. (Color) Average reflectivity as a function of d_1 and ω at $\omega_p=0.8$ eV.

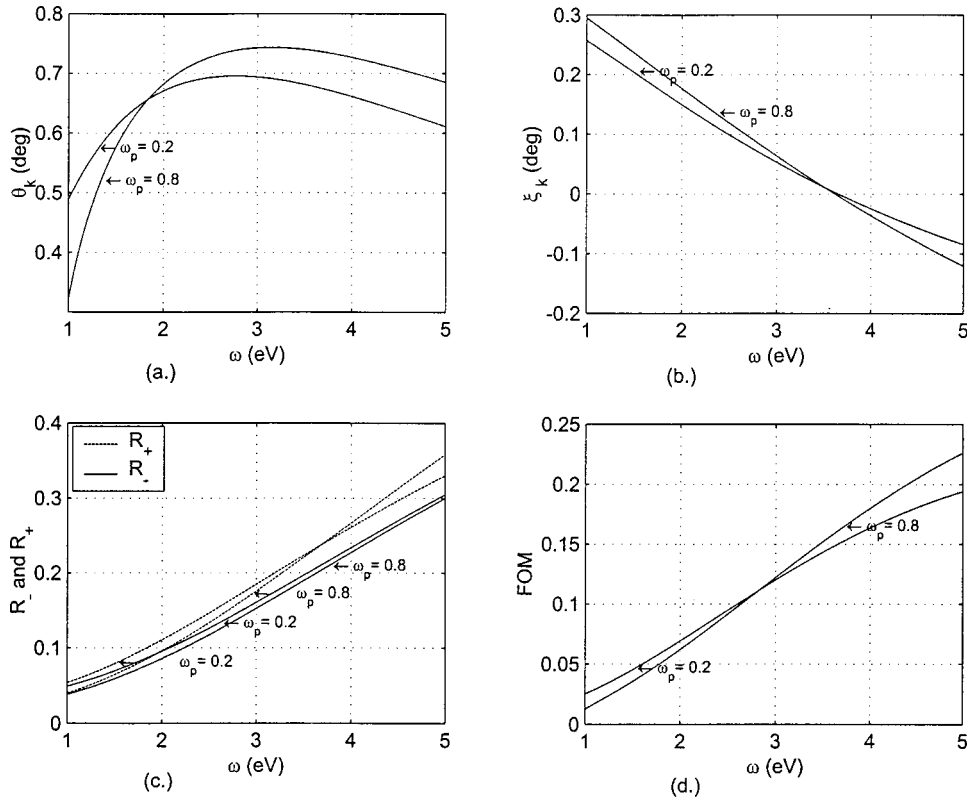


FIG. 5. (a) Kerr rotation (b) Kerr ellipticity, (c) reflectivity, and (d) FOM for 013 with $d_1 = 4.5$ nm.

Figure 1 shows the real and imaginary parts of the cyclotron frequency for InSb for various values of plasma frequency. The optical constants for InSb were obtained from Ref. 17. As can be quite clearly seen from Fig. 1, the maximum value of plasma frequency for this material has to be around 0.9 eV so as to keep ω_c real.

III. 2x2 CHARACTERISTIC MATRIX FORMULATION

In order to analyze the spectra of the complex MO Kerr spectra of a multilayer system, a 2x2 MO characteristic matrix is employed. The characteristic transfer matrix for N number of parallel, homogeneous, isotropic layers can be given by

$$\begin{bmatrix} \tilde{S}_{11}^\pm & \tilde{S}_{12}^\pm \\ \tilde{S}_{21}^\pm & \tilde{S}_{22}^\pm \end{bmatrix} = \prod_{i=1}^N \frac{1}{\tilde{t}_{i,i+1}^\pm} \begin{bmatrix} e^{j\beta_i^\pm} & 0 \\ 0 & e^{-j\beta_i^\pm} \end{bmatrix} \times \begin{bmatrix} 1 & \tilde{r}_{i,i+1} \\ \tilde{r}_{i,i+1} & 1 \end{bmatrix}. \quad (16)$$

In the polar Kerr configuration the magnetization is perpendicular to the surface and parallel to the direction of light propagation. The eigenmodes are left and right circular polarizations and thus the Fresnel's reflection and transmission coefficients at normal incidence of each interface is given by

$$\tilde{r}_{i,i+1}^\pm = \frac{n_i^\pm - n_{i+1}^\pm}{n_i^\pm + n_{i+1}^\pm}$$

and

$$\tilde{t}_{i,i+1}^\pm = \frac{2n_i^\pm}{n_i^\pm + n_{i+1}^\pm}. \quad (17)$$

The phase factor is given by $\beta_i^\pm = (2\pi/\lambda)n_i^\pm d_i$, where d_i is the thickness of the i th layer.

The complex reflection coefficient of the multilayer system can be obtained from the resultant characteristic transfer matrix

$$r_r^\pm = \frac{\tilde{S}_{21}^\pm}{\tilde{S}_{11}^\pm}. \quad (18)$$

The reflectivity is given by

$$R_\pm = |r_r^\pm|^2. \quad (19)$$

KR can also be expressed as the phase difference between left and right circularly polarized light¹⁸

$$\theta_K = -\frac{1}{2}(\Delta_+ - \Delta_-), \quad (20)$$

where the phase difference is given by

$$\begin{aligned} \Delta_\pm &= \tan^{-1} \left(\frac{-2k_\pm}{n_\pm^2 + k_\pm^2 - 1} \right) \\ &= -j \log \frac{r_r^\pm}{|r_r^\pm|}. \end{aligned} \quad (21)$$

KE can simply be expressed in terms of reflection coefficients as

$$\xi_K = -\frac{|r_+| - |r_-|}{|r_+| + |r_-|}. \quad (22)$$

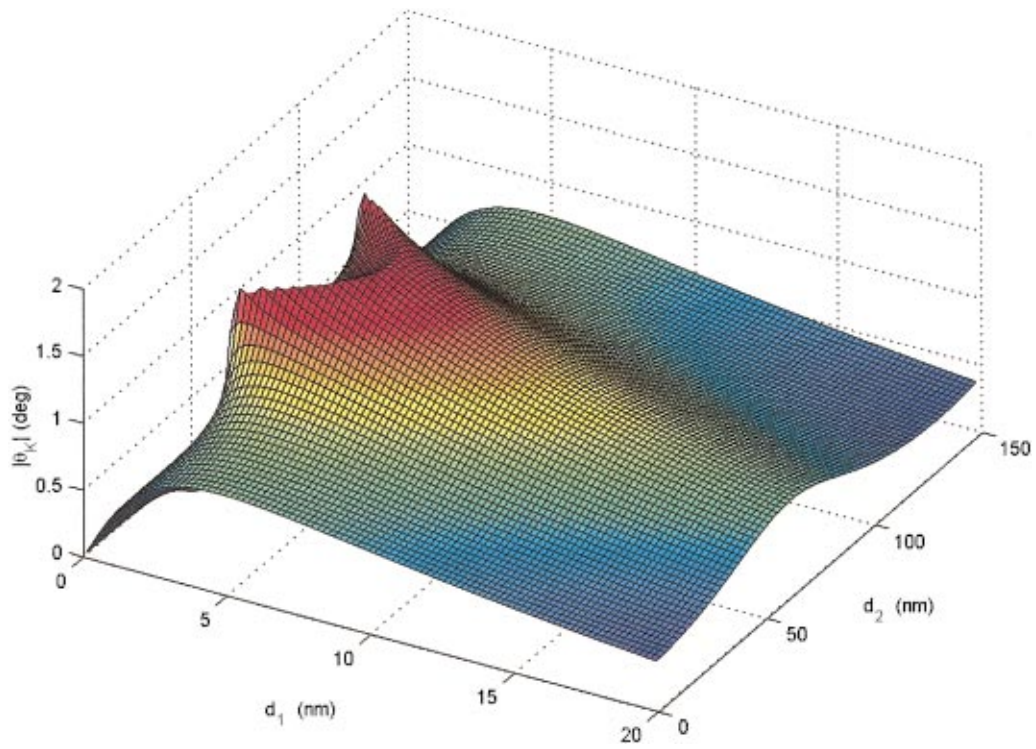


FIG. 6. (Color) Kerr rotation as a function of d_1 and d_2 at $\omega = 3.1$ eV and $\omega_p = 0.8$ eV.

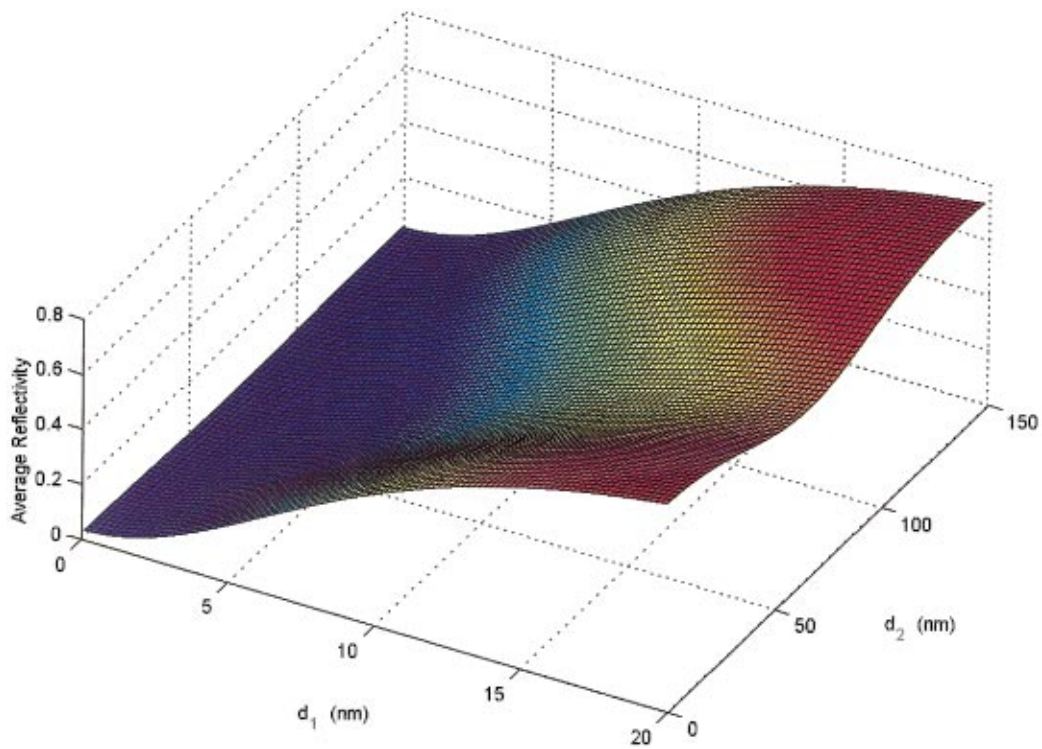


FIG. 7. (Color) Average reflectivity as a function of d_1 and d_2 at $\omega = 3.1$ eV and $\omega_p = 0.8$ eV.

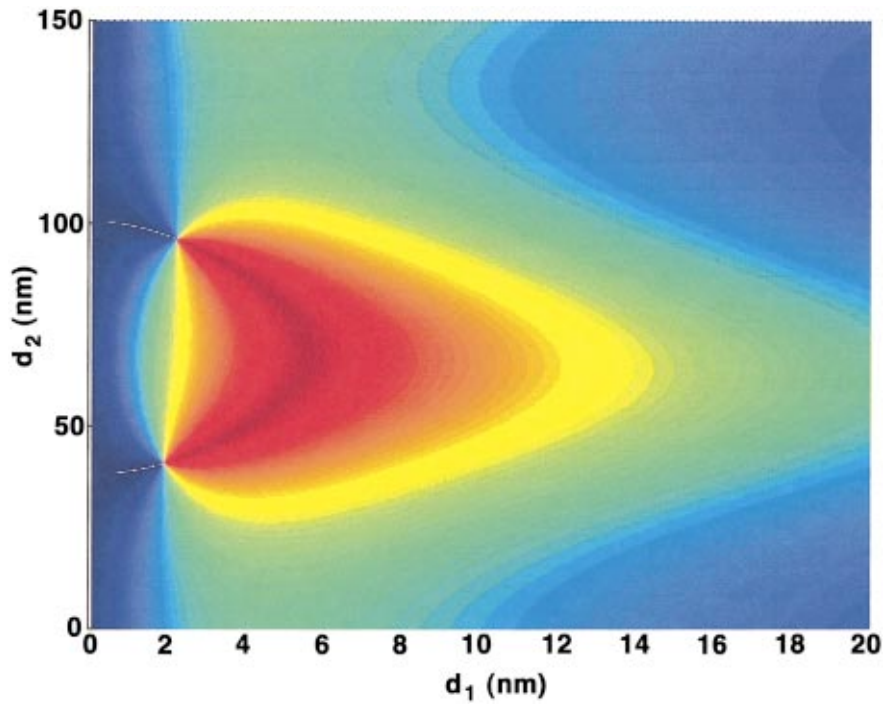


FIG. 8. (Color) Color contours of constant Kerr rotation as a function of d_1 and d_2 at $\omega = 3.1$ eV and $\omega_p = 0.8$ eV.

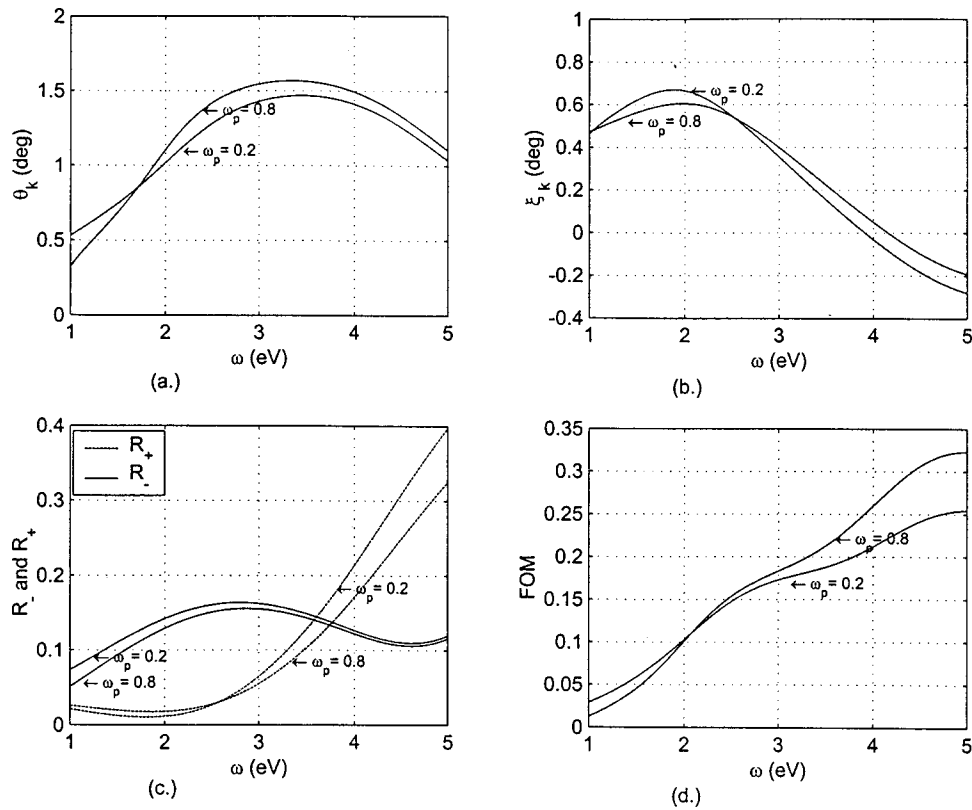


FIG. 9. (a) Kerr rotation, (b) Kerr ellipticity, (c) reflectivity, and (d) FOM for 0213 bilayer stack with $d_1 = 5$ nm and $d_2 = 56$ nm.

TABLE I. Comparison of MOKE parameters for various configurations at $\omega = 3.1$ eV and $\omega_p = 0.8$ eV.

Configuration	d_1 (nm)	d_2 (nm)	θ_K (deg)	ξ_K (deg)	R_+	R_-	R_{avg}	FOM
01	—	—	0.269	-0.625	0.994	0.349	0.672	0.200
013	4.5	—	-0.743	0.053	0.184	0.159	0.171	0.128
0213	5	56	1.563	0.274	0.087	0.152	0.119	0.544

A FOM may be used to characterize the performance of a multilayer MO media.¹⁴ While evaluating several MO material systems, the FOM can be used as a basis for quantitative comparison. It can be expressed as

$$\text{FOM} = \sqrt{\theta_K^2 \cdot R_a}, \quad (23)$$

where R_a is the average reflectivity and is given by $R_a = |r_+^2| + |r_-^2|$.

IV. NUMERICAL RESULTS AND DISCUSSION

The numbers 0, 1, 2, 3 are assigned to air, MO semiconductor material (InSb), low refractive index DE material, and substrate, respectively. The low refractive index DE material chosen was LiF and SiO₂ was chosen to be the substrate. We are justified in choosing a low refractive index material as a substrate. It has been shown⁹ that if the nonmagnetic reflector has a low refractive index then an enhancement of KR is achieved. Material dispersions were taken into account and the refractive indices for LiF and SiO₂ in the 1–5 eV regions were obtained from Ref. 17. In the optical frequency range of 1–5 eV, the refractive indices of the InSb were calculated using Eqs. (5), (9), and (13). The optical constants for InSb are:¹⁷ $\epsilon_\infty = 15.7$, $\omega_L = 19$ meV, $\omega_T = 17$ meV, $\Gamma = 1.2$ meV, and $\gamma = 0.6$ meV.

In Fig. 2 we plot various MOKE parameters for bulk MO media (01 configuration) as a function of optical frequency and for various ω_p values. The reflection coefficients are calculated using Eqs. (15) and (16). The KR as seen from Fig. 2 is in general higher for the higher ω_p value. At $\omega_p = 0.8$ eV, the KR has a quadratic variation with respect to the optical frequencies, it is 0.355° at 1 eV and then gradually flattens out to 0.266° at 5 eV. The higher KR value of 0.355° at 1 eV is due to the close proximity of the plasma resonance edge. The KE also exhibits a quadratic behavior and is -0.662° at 1 eV and goes down to -0.621° at 5 eV. With $\omega_p = 0.2$ eV, the MOKE parameters vary more linearly since the plasma resonance edge would be further away from the spectral region under observation, as compared to the $\omega_p = 0.8$ eV case. KR is about 0.2635° throughout; KE varies from -0.608° to -0.533° .

The effect of depositing a thin film of InSb on a SiO₂ substrate (013 configuration) is studied next. A three dimensional (3D) graph showing the effect of varying ω and d_1 on the KR can be seen in Fig. 3, where at higher optical frequencies the KR peaks for a film thickness of about $d_1 = 4.5$ nm. It is worth noting that the value of d_1 at which maximum KR occurs increases rapidly as we move to lower optical frequencies. The corresponding average reflectivity is shown in Fig. 4. We can observe from the figures that the highest average reflectivity corresponds to the lowest KR value, however the converse is not necessarily true.

In Fig. 5 by setting the film thickness to the optimized value of 4.5 nm we plot various MOKE parameters for different values of ω_p . The resulting reflectivity and FOM are quite low in this case. The peak KR was 0.743° at about 3.1 eV and for $\omega_p = 0.8$ eV. The corresponding KE was 0.042° , and R_+ and R_- are 19.32%, and 16.7% respectively. The KR for $\omega_p = 0.8$ eV displays impressive broadband characteris-

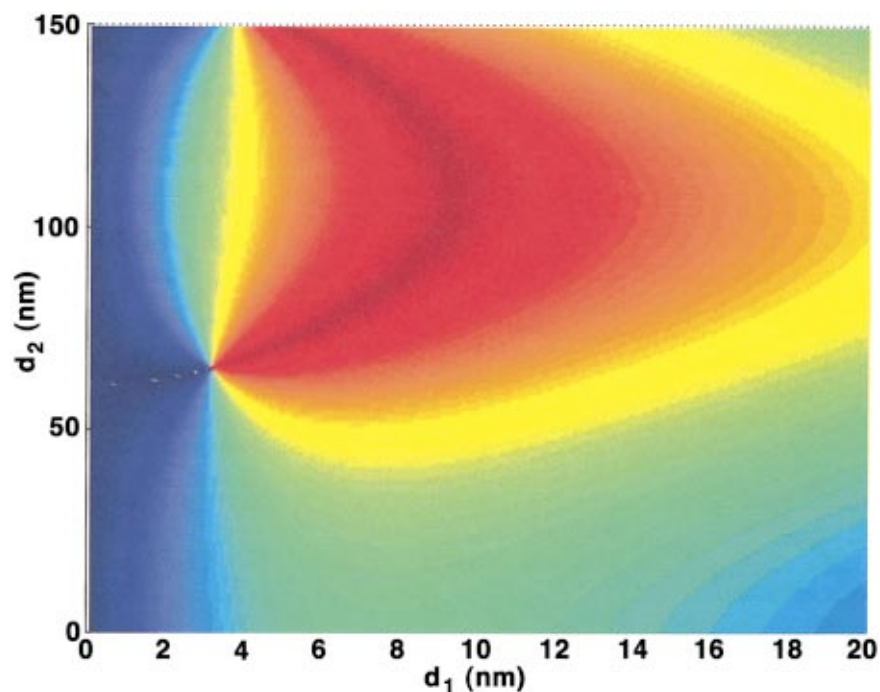


FIG. 10. (Color) Color contours of constant Kerr rotation as a function of d_1 and d_2 at $\omega = 2$ eV and $\omega_p = 0.8$ eV.

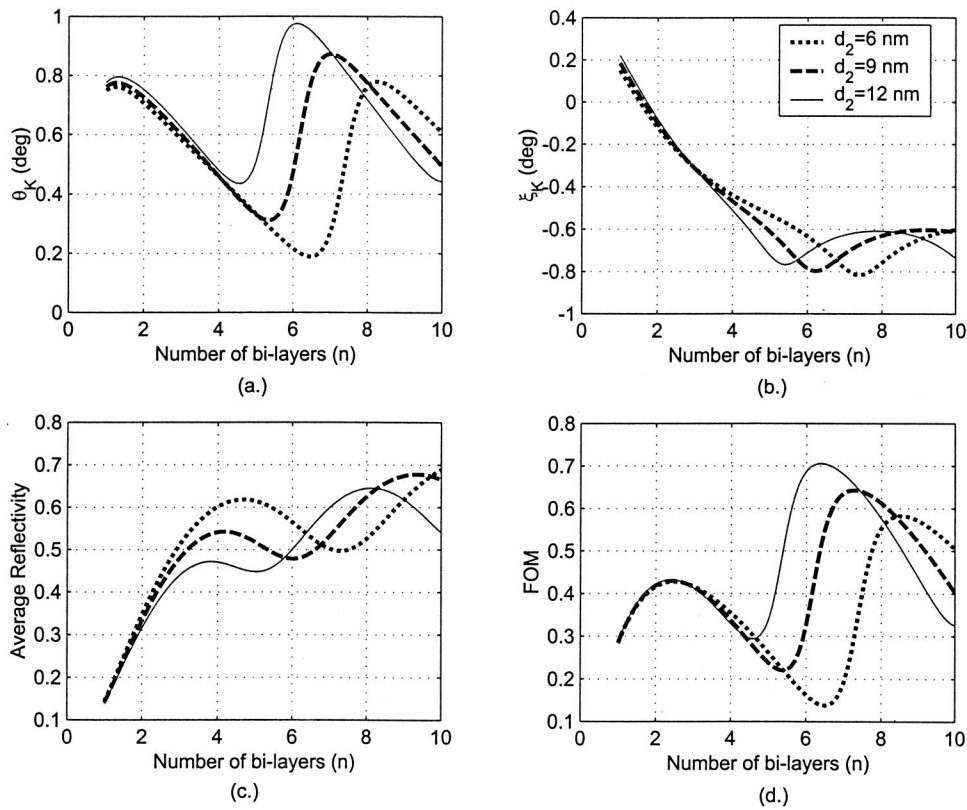


FIG. 11. (a) Kerr rotation, (b) Kerr ellipticity, (c) reflectivity, and (d) FOM for 0(21)ⁿ3 as a function of *n* at $\omega = 3.1$ eV, $\omega_p = 0.8$ eV, and $d_1 = 4$ nm.

tics and is greater than 0.7° between 2.15 and 4.67 eV. The KR for most part of the spectrum is higher for $\omega_p = 0.8$ eV than for $\omega_p = 0.2$ eV. However, at 1.836 eV they are both equal and below 1.836 eV, $\omega_p = 0.2$ eV yields a higher KR.

A further improvement in the KR is seen in the 0213 configuration where a thin film of a low refractive material (LiF) is deposited on the input side. The KR is expected to increase and is also usually accompanied by an enhancement in KE. This is due to the fact that the polarized light beam would experience multiple reflections and interference effects in the DE layer. A low refractive index DE would reduce the polarization component of the directly reflected light without influencing the component induced by the KR. This would thus aid in the enhancement of KR.

TABLE II. MOKE related parameters obtained after optimizing FOM for 0(21)ⁿ3 layers at $\omega = 3.1$ eV and $\omega_p = 0.8$ eV.

<i>n</i>	<i>d</i> ₁ (nm)	<i>d</i> ₂ (nm)	θ_K (deg)	ξ_K (deg)	<i>R</i> ₊	<i>R</i> ₋	<i>R</i> _{avg}	FOM
1	5	56	1.563	0.274	0.087	0.152	0.119	0.544
2	10.9	61.7	1.570	-0.378	0.735	0.619	0.677	1.329
3	12.3	63.5	1.566	-0.448	0.886	0.843	0.865	1.515
4	12.7	62.8	1.571	-0.466	0.929	0.915	0.922	1.573
5	12.9	62.2	1.571	-0.472	0.944	0.945	0.944	1.594
6	13.0	62.1	1.571	-0.472	0.948	0.964	0.956	1.604
7	13.0	62.9	1.571	-0.467	0.945	0.983	0.964	1.609
8	13.1	62.0	1.569	-0.471	0.951	0.983	0.967	1.611
9	13.1	62.2	1.570	-0.469	0.950	0.989	0.969	1.614
10	13.1	62.3	1.570	-0.469	0.950	0.993	0.971	1.615

A 3D profile view of KR and reflectivity as a function of thickness and for $\omega = 3.1$ eV (400 nm) and $\omega_p = 0.8$ eV can be seen in Figs. 6 and 7, respectively. The highest reflectivity corresponds to the lowest KR, however, and as stated earlier the converse is not necessarily true. A color contour plot of the KR was plotted and is shown in Fig. 8. This was done in order to determine the *d*₁ and *d*₂ values that yield the highest KR. The dark red and the blue regions correspond to the highest and lowest KR values, respectively. This figure leads us to a choice of *d*₁ = 5 nm or *d*₂ = 56 nm to optimize KR. Note the KR and the average reflectivity are periodic with respect to layer thickness and that there exist multiple solutions of *d*₁ and *d*₂ that would yield identical results. We select the lowest possible values of *d*₁ and *d*₂.

TABLE III. MOKE related parameters obtained after optimizing FOM for 0(21)ⁿ3 layers at $\omega = 3.1$ eV and $\omega_p = 2.4$ eV.

<i>n</i>	<i>d</i> ₁ (nm)	<i>d</i> ₂ (nm)	θ_K (deg)	ξ_K (deg)	<i>R</i> ₊	<i>R</i> ₋	<i>R</i> _{avg}	FOM
1	10.0	67.1	1.497	-0.043	0.220	0.123	0.172	0.620
2	16.9	60.5	1.571	-0.409	0.767	0.587	0.677	1.336
3	19.0	61.8	1.568	-0.473	0.920	0.823	0.872	1.529
4	19.6	61.4	1.569	-0.490	0.966	0.911	0.939	1.593
5	19.9	63.2	1.570	-0.486	0.971	0.968	0.969	1.619
6	20.0	60.9	1.571	-0.497	0.989	0.971	0.980	1.631
7	20.1	60.3	1.570	-0.497	0.992	0.979	0.985	1.635
8	20.1	60.8	1.570	-0.496	0.992	0.989	0.990	1.639
9	20.1	61.1	1.571	-0.495	0.992	0.994	0.993	1.641
10	20.1	61.3	1.571	-0.495	0.992	0.996	0.994	1.642

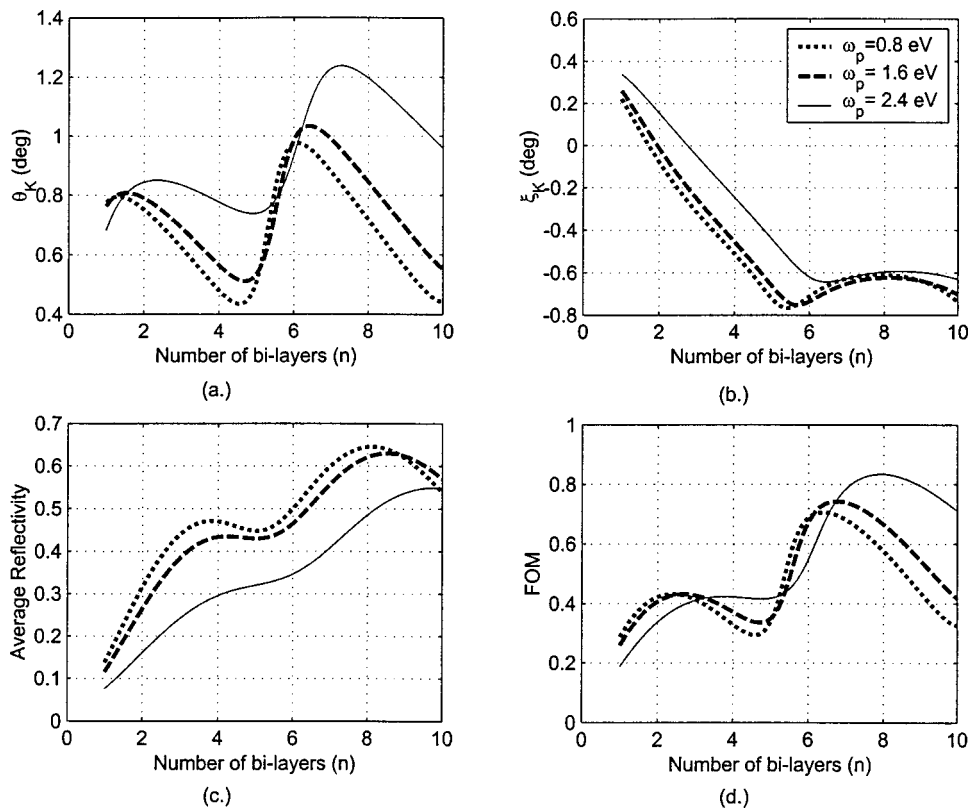


FIG. 12. (a) Kerr rotation, (b) Kerr ellipticity, (c) reflectivity, and (d) FOM for $0(21)^n3$ as a function of n at $\omega = 3.1$ eV, $d_1 = 4$ nm, and $d_2 = 12$ nm.

Using the d_1 and d_2 values obtained from above we plot various MOKE parameters for the 0213 configuration in Fig. 9. We see that the KR at 1.71 eV is the same for both values of ω_p . Above the 1.71 eV mark, however, $\omega_p = 0.8$ eV yields a higher KR and is at least 1.4° over a relatively broad range of optical frequencies between 2.45 and 4.32 eV. The peak KR is 1.563° and the corresponding KR is 0.274° at 3.1 eV. The reflectivity for R_+ and R_- is 8.7% and 15.18%, respectively. R_+ remains below 20% below the 4 eV mark for $\omega_p = 0.8$ eV. However, its increase is more rapid for the lower ω_p value of 0.2 eV. The KR and KE for this particular configuration has certainly been enhanced over the 013 case. As an illustration, a comparison among the 01, 013, and 0213 configuration MOKE parameters at $\omega = 3.1$ eV and $\omega_p = 0.8$ eV has been shown in Table I. Notice an enhancement of nearly 100% as we go from the 013 to the 0213 configuration.

In Fig. 10 we set $\omega = 2$ eV and look for d_1 and d_2 to yield optimum KR. After comparing this against Fig. 8 and by looking at a number of other cases with different ω values we conclude that higher thickness for both d_1 and d_2 is required in order to optimize KR at lower optical frequencies and vice versa.

One obvious drawback of the simple bilayer structure is its low average reflectivity and hence low FOM. By repeating the LiF and InSb bilayers a number of times, i.e., a $(21)^n3$ configuration, the FOM can be significantly improved.

We would like to briefly discuss some general behavioral aspects of this. In Fig. 11, various MO parameters have been

plotted as a function of n for given d_1 and d_2 values, which were arbitrarily chosen to emphasize the following characteristics. We set $d_1 = 4$ nm and $d_2 = 12, 9, 6$ nm. Note that the KR and reflectivity are nonlinear and have a complex oscillatory behavior with respect to n . We have only shown the first oscillation for our present discussion. Also note that the FOM is nearly indistinguishable and insensitive to changes in d_2 up to $n = 4$, beyond which it is seen that the higher d_2 value yields a higher FOM. In addition this is achieved for fewer repetitions of the bilayer. The value of n over which the FOM remains indistinguishable depends on the choice of d_1 and is inversely proportional to it. This was concluded by looking at various cases with different d_1 values.

In Table II we provide the optimized d_1 and d_2 thickness values for a given n , which yields maximum FOM (at $\omega_p = 0.8$ eV and $\omega = 3.1$ eV). Between $n = 1$ and $n = 2$, there is a significant jump in the reflectivity and hence FOM. At $n = 4$, the average reflectivity is more than 90% and FOM is 1.573 and from there on, for even higher values of n , the increase in the FOM is quite small. Also note that d_1 and d_2 do not vary much and beyond $n = 4$ and they too tend to saturate with increasing n . Similar trends are observed in Table III, which is calculated at $\omega_p = 2.4$ eV and $\omega = 3.1$ eV. No improvements in KR and only minor improvements in FOM were noted. Also the thickness of d_1 required to optimize the FOM was higher in the case of the higher plasma frequency, however the d_2 requirements remained essentially the same at about 60 nm. We conclude that due to the ω_c condition set by Eq. (13), the proximity to the plasma edge would not yield much in terms of Kerr rotation once the

thickness of the individual layers has been optimized. Thus under the present set conditions any error in the doping level may be compensated by changing the MO layer thickness. Notice that there is an enhancement of about 200% in the FOM as we go from $n=2$ to $n=4$.

Figure 12 gives the MOKE parameters at 3.1 eV for various values of ω_p by setting $d_1=4$ nm and $d_2=12$ nm. These were chosen to demonstrate some MOKE behavioral trends, at arbitrary layer thickness, as the material's doping concentration is changed. The initial indistinguishable features of Fig. 11 are not there. It is seen that for $\omega_p=0.8$ and 1.6 eV, a FOM of about 0.42 is achieved for $n=2$ whereas for $\omega_p=2.4$ eV, four bilayers are required to give the same result. However the contribution due to ω_p is more significant as we move on to a higher number of layers. Expect for $n=1$, the KR for $\omega_p=2.4$ is significantly higher in general. Hence we can conclude that at arbitrary MO layer thickness and at higher values of n , the proximity of the plasma resonance to the incident photon energy does make a significant difference.

V. SUMMARY

In this work, the plasma resonance condition for free charge carriers (i.e., $\text{Re}[\epsilon_{xx}]=1$) was extended to a broad range of optical frequencies by appropriate coupling of ω and ω_c , for fixed ω_p . It is observed that a ω_c - coupled MO layer could be made to peak at a particular optical frequency by the appropriate choice of DE and MO layer thickness. In general higher ω_p values resulted in higher KR. We would like to point out some similar findings in the literature. KR values in the case of MnBi were reported as 0.7^{08} and 2.0^{18} for the same optical frequency. These differences have been attributed to the doping densities and the band structure of the MO medium, which in turn is related to their respective

dielectric-tensor properties. For several applications such as design of MO storage media, high KR alone is not sufficient. One needs to improve the reflectivity. We have shown this to be achievable at 3.1 eV by making several repetitions of the MO/DE bilayer. The most economical choice if one desires average reflectivity greater than 90% along with high KR is the $0(21)^n3$ design with $n=4$ as shown in Table I. As a further extension of the present work, the role of interplay between ω_c and ω_p (in addition to the plasma resonance condition) in a Kerr enhancement mechanism is currently being investigated.

¹H. S. Bennet and E. A. Stern, Phys. Rev. **137**, A448 (1965).

²J. L. Erskine and B. R. Cooper, Phys. Rev. B **8**, 1239 (1973).

³H. Fiel and C. Haas, Phys. Rev. Lett. **58**, 65 (1987).

⁴T. Katayama, Y. Suzuki, H. Awano, Y. Nishihara, and N. Koshizuka, Phys. Rev. Lett. **60**, 1426 (1988).

⁵J. Ferre *Proceedings of the Conference on Magnetism, Magnetic Materials and their Applications*, La Habbna, Cuba 1991 (IOP, Berkshire, 1992).

⁶V. I. Safarov, V. A. Kosobukin, C. Hermann, G. Lampel, and J. Peretti, Phys. Rev. Lett. **73**, 3584 (1994).

⁷R. Fang, C. Peng, T. Ma, P. Long, J. Liu, Y. Nin, and D. Dai, J. Appl. Phys. **74**, 11 (1993).

⁸W. Reim and D. Weller, Appl. Phys. Lett. **53**, 2453 (1988).

⁹A. Hubert and G. Traeger, J. Magn. Magn. Mater. **24**, 185 (1993).

¹⁰L. Y. Chen, W. A. McGahan, Z. S. Shan, D. J. Sellemeyer, and J. A. Woolam, J. Appl. Phys. **67**, 5337 (1990).

¹¹D. O. Smith, Opt. Acta **12**, 13 (1965).

¹²R. Nies and F. R. Kessler, Phys. Status Solidi A **111**, 639 (1989).

¹³M. Mansuripur, J. Appl. Phys. **67**, 6466 (1990).

¹⁴W. Reim and J. Schones *Magneto Optical Spectroscopy, Ferromagnetic Materials (Elsevier Science, New York, 1990)*, Vol. 5.

¹⁵S. J. Buchsbaum, *Proceeding of the International Conference on the Physics of Semiconductors, Symposium on Plasma Effect in Solids* (Dunod, Paris, 1964).

¹⁶P. Drude, *The Theory of Optics (Tuebrer Leipzig 1900)* (Dover, New York, 1959).

¹⁷*Handbook of Optical Constants of Solids*, edited by E. D. Palik (Academic, New York, 1996).

¹⁸K. Egashira and T. Yamada, J. Appl. Phys. **45**, 3643 (1974).